# Shaking stack model of ion conduction through the $Ca^{2+}$-activated $K^+$ channel

Mark F. Schumaker
Department of Pure and Applied Mathematics, Washington State University, Pullman, WA 99164-3113 USA

ABSTRACT Motivated by the results of Neyton and Miller (1988. *J. Gen. Physiol.* 92:549–586), suggesting that the $Ca^{2+}$-activated $K^+$ channel has four high affinity ion binding sites, we propose a physically attractive variant of the single-vacancy conduction mechanism for this channel. Simple analytical expressions for conductance, current, flux ratio exponent, and reversal potential under bi-ionic conditions are found. A set of conductance data are analyzed to determine a realistic range of parameter values. Using these, we find qualitative agreement with a variety of experimental results previously reported in the literature. The exquisite selectivity of the $Ca^{2+}$-activated $K^+$ channel may be explained as a consequence of the concerted motion of the "stack" in the proposed mechanism.

## INTRODUCTION

The high conductance $Ca^{2+}$-activated $K^+$ (CaK) channel exhibits a remarkable combination of very high conductance for $K^+$ and strong selectivity in favor of $K^+$ over other cations. The conductance may be resolved into a rate of ion entrance into the channel and a subsequent rate of permeation through the channel and exit thereafter (Latorre and Miller, 1983). The entrance rate may be high in part due to negatively charged groups on the protein near the mouth of the channel (MacKinnon et al., 1989). The second component of conductance is responsible for the high value of $\gamma_{max}$ measured for the CaK channel, that is, the apparent saturating value of conductance measured at high ion activities. One early proposal to explain this high value envisioned a multi-ion channel. The entry of a second ion into the conduction pore from one side of the membrane would provide the electrostatic repulsion to "push" the first ion out (Andersen and Procopio, 1980; Läuger, 1980). Indeed, the high conductance CaK channel from rat muscle T-tubules was subsequently found to be a multi-ion channel (Eisenman et al., 1986).

The single-filing region of the rat muscle CaK channel has been found more recently to contain four ion binding sites with a very high affinity for $K^+$ (Neyton and Miller, 1988*a*, *b*). At least three of these would always be occupied at physiological $K^+$ concentrations. The Gárdos $K^+$ channel from human red blood cells (Gárdos, 1958) also appears to be an "ion-avid" channel. The flux ratio exponent for this channel was found to have an essentially constant value of $n \approx 2.7$ over a wide range of $K^+$ concentrations (intracellular 30–145 mM, extracellular 1–150 mM) and transmembrane potentials (Vestergaard-Bogind et al., 1985; Stampe, P., personal communication), demonstrating that the ion occupancy of this channel does not decrease as the ion activities in the surrounding media are lowered.

Motivated by these observations, Schumaker and MacKinnon (1990) introduced the "single-vacancy" model for ion conduction: if a channel has $m$ ion binding sites along its conduction pore, they are occupied by either $m$ or $m - 1$ ions. Hydrating waters and chemical groups within the pore would be required to electrically neutralize or disperse the concentrated charge of the conducting ions. The single-vacancy feature of the model greatly reduces the number of states that need to be considered for the calculation of certain measurable properties. By further specializing the analysis to a four-parameter "simple pore" model of the channel, simple analytical expressions were found for the current and conductance, as well as the low and high activity limits of the permeability ratio.

This paper proposes a conduction mechanism of the CaK channel that is a physically attractive limit of single-vacancy conduction—the "shaking stack" model (Schumaker, 1991). We imagine that the $m$ ion binding sites have associated with them a "stack" of $m$ or $m - 1$ ions, including waters of hydration. An ion from solution may join a stack of $m - 1$ ions at the vacant binding site, and an ion may escape into solution from either end of a stack of $m$ ions. The stack of $m - 1$ ions may also make a concerted transition from the first $m - 1$ binding sites to the last $m - 1$ sites within the conduction pore. The concerted motion feature of this model is a simple way to fulfill the requirement that the movement of an ion in a condensed phase be coordinated with the motion of the ions and molecules in its neighborhood. Concerted motion of the stack is also easily seen to magnify selectivity differences between permeant ions. By again considering a simple pore, we will be able to find simple formulas for the current, conductance, permeability ratio and flux ratio exponent.

We also analyze a set of conductance data to determine the range of parameter values required to mimic the properties of the CaK channel. Using Neyton and Miller's finding that there are four ion binding sites in the rat muscle CaK channel, only three further simple pore parameter values are required. These are partially determined by the available data. Four sets of parameters are considered that typify the remaining range of possibilities. Two of these sets can account qualitatively for measurements of the current, conductance, and permeability ratio previously reported in the literature. A


0006-3495/92/10/1032/13 $2.00

partial explanation also can be given for the observed properties of the flux ratio exponent of the Gárdos channel.

## MATERIALS AND METHODS

Plasma membrane vesicles containing CaK channels were prepared from rat skeletal muscle as described by Moczydlowski and Latorre (1983). The lipids used were 1-palmitoyl,2-eleoyl phosphatidylethanolamine (POPE) and the analogous phosphatidyl choline (POPC), obtained from Avanti Polar Lipids, Inc. (Birmingham, AL). CaK channels were inserted into the planar lipid bilayers as described previously (Latorre et al., 1982; Miller, 1987). Bilayers were formed by applying a drop of lipid solution (14 mM POPE + 6 mM POPC in *n*-decane) to a 250-$\mu$m-diameter hole in the plastic septum separating the two chambers filled with aqueous solution (10 mM *N*-2-hydroxyethylpiperazine-*N'*-2-ethane sulfonic acid, 5 mM *N*-methyl-D-glucamine (NMDG), and varying concentrations of KCl as described in the results; pH 7.4). A final addition of $CaCl_2$ was made to the "internal chamber" (final concentration 200 $\mu$M) to activate the CaK channels. CaK channel conductances were measured in symmetrical KCl solutions by measuring the slope of I-V curves generated by voltage ramps centered at zero-applied potential. KCl activities were computed from concentrations by means of activity tables.

## RESULTS

Measurements of CaK conductance as a function of symmetrical $K^+$ activity are shown as the filled circles in Fig. 1 *a*. These data may be plotted in an alternative way as suggested by the single-vacancy model of ion conduction (Schumaker and MacKinnon, 1990). According to that model, the conductance, $\gamma$, will depend on the $K^+$ activity, $x$, with the general form

$$\gamma = \frac{e^2}{k_B T} \frac{x}{A + Bx + Cx^2}, \qquad (1)$$

where $e$ is the elementary electrical charge, $k_B$ is Boltzmann's constant, and $T$ is the absolute temperature. The constants $A$, $B$, and $C$ are model dependent. Solving for $x/\gamma$, one obtains

$$\frac{x}{\gamma} = \frac{k_B T}{e^2}(A + Bx + Cx^2). \qquad (2)$$

Replotting the data with $x/\gamma$ as a function of $x$, we obtain Fig. 1 *b*.

A straight line fit through the five data points at the higher activities was made by means of an unweighted least-squares analysis. The values obtained for the slope and intercept are $A = 1.87\ 10^{-9}$ M s and $B = 8.17\ 10^{-9}$ s. The solid line in Fig. 1 *b* shows this result. Corresponding values of $\gamma$ are obtained from Eq. 1, with the quadratic term in the denominator left out. They are plotted as the solid curve in Fig. 1 *a*. The two data points at low activity show an anomalously high conductance. This may be due to surface charges near the channel mouth (MacKinnon et al., 1989), and these points are excluded from the least-squares analysis.

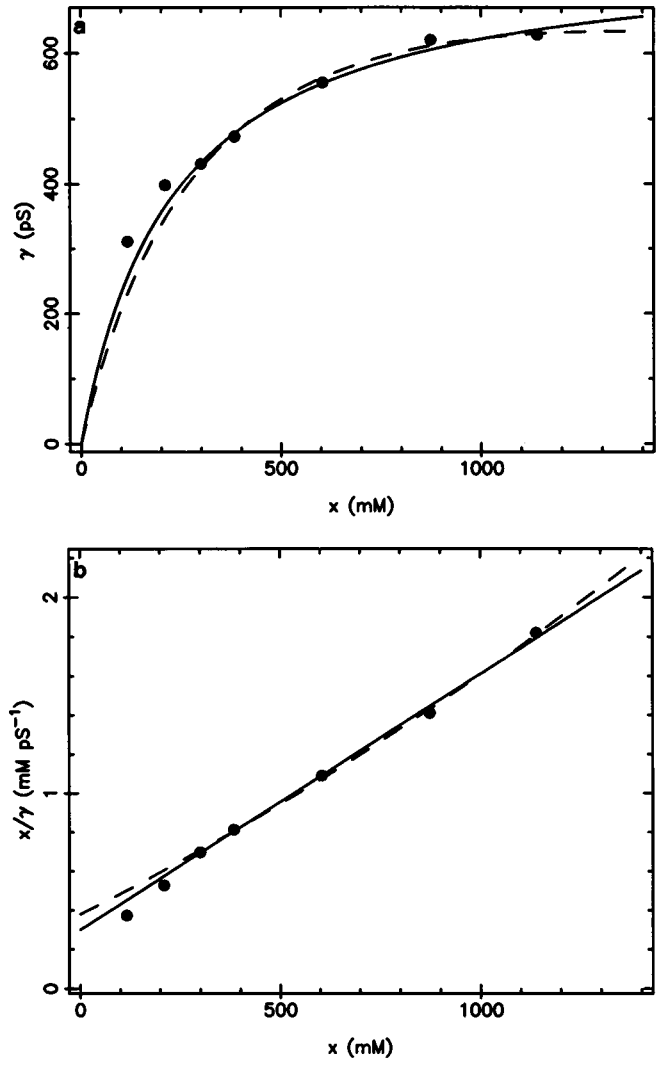


FIGURE 1 (*a*) Channel conductance, $\gamma$, plotted as a function of symmetrical $K^+$ activity, $x$. Filled circles show observations. The solid line is a rectangular hyperbola with parameters obtained from a linear least-squares analysis of the data in *b*. The dashed line corresponds to Eq. 1 with parameters determined by a quadratic least-squares analysis of the data in *b*. (*b*) Data are replotted according to Eq. 2 to show a linear trend. The linear least-squares analysis of the five data points at high activity is shown as the solid line. The quadratic analysis of these data is shown as the dashed line.

In addition to the linear analysis of the data in Fig. 1 *b*, a quadratic least-squares analysis of the $x/\gamma$ values also has been made. Optimal coefficients for Eq. 2 are $A = 2.37\ 10^{-9}$ M s, $B = 6.43\ 10^{-9}$ s, and $C = 1.23\ 10^{-9}$ $M^{-1}$ s. The dashed curves in Fig. 1, *a* and *b* show the corresponding values of $\gamma$ and $x/\gamma$. The term $Cx^2$, which is responsible for the curvature of the dashed line in Fig. 1 *b*, also leads to a maximum conductance at activity $x = (A/C)^{1/2} \approx 1.4$ M. Increasing CaK conductances have been measured up to concentrations of 2 M KCl (see also Villarroel and Eisenman, 1987), corresponding to an activity of ~1,140 mM. Assuming that the form of Eq. 1 is correct, the absence of an observed conductance

maximum suggests that the value of $C$ just obtained must represent an approximate upper bound of the "true" value. Therefore, the values for $A$, $B$, and $C$ found by means of the quadratic least-squares analysis and the corresponding rate constants obtained in the Analysis of Conduction Data, below, will be referred to as the high curvature parameters.

Both the linear and quadratic fits discussed above are compatible with the data shown in Fig. 1. We therefore obtain a second set of parameters that is closer to the linear analysis. The data in Fig. 1 *b* are fit with another quadratic polynomial, where a specified value of $C = 1.23\ 10^{-10}\ M^{-1}$ s is required, this being a factor of 10 smaller than that found for the high curvature parameters. Least-squares values of $A = 1.92\ 10^{-9}$ M s and $B = 7.99\ 10^{-9}$ s are obtained under this constraint. These values, and the rate constants calculated from them, will be referred to as the low curvature parameters below. They yield a fit to the data very close to the solid line in Fig. 1, *a* and *b*.

## SHAKING STACK MODEL

The transformation of conductance data given in Eq. 2 and carried out in Fig. 1 *b* is suggested by the single-vacancy model of ion conduction (Schumaker and MacKinnon, 1990). In this section we describe a special limit of single-vacancy conduction, the shaking stack, which is a physically attractive model for the conduction mechanism of the CaK channel.

Fig. 2 *a* schematically portrays the shaking stack mechanism. Within the single-filing region of the conduction pore, the motion of ions and their associated waters of hydration are assumed to be tightly coupled, forming a "stack." Ions may be gained or lost from the stack only singly, at its ends. Consistent with the results of Neyton and Miller (1988*a*, *b*) on the occupation of binding sites within the pore of the CaK channel, the figure shows a stack of three ions associated with three binding sites and a fourth site vacant (occupied by water molecules). An important degree of freedom allows the stack to shift from the first three binding sites to the last three, translocating the vacancy from one end of the stack to the other. Conduction occurs when an ion from solution occupies a vacant binding site at one end of the stack, allowing an ion from the other end to come off (as suggested by the figure). The original configuration is restored by a single shift of the stack.

The synchronous motion of the ions comprising the stack may at first seem to require special justification. However, movement of an ion in a condensed phase must be coupled with the coordinated motion of a different ion or molecule into the space that the first ion originally occupied. When a vacancy is created by the motion of an ion in the interior of the pore, there are three ways that it may be filled. (*a*) The first possibility is that the ion exchanges position with a water molecule. This

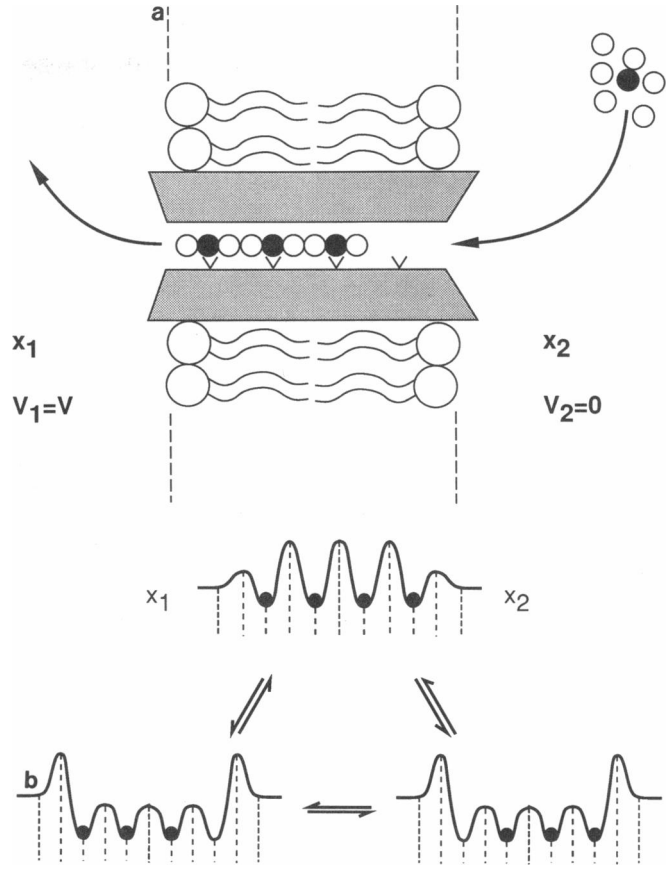


FIGURE 2 (*a*) Illustration of the shaking stack conduction mechanism. Channel protein is embedded in a lipid bilayer separating aqueous solutions. Side 1 has ion activity $x_1$ and applied electrical potential $V_1 = V$. Side 2 has activity $x_2$ and potential $V_2 = 0$. The conduction mechanism is described in the text. (*b*) Potential profiles of the three states of the shaking stack conduction mechanism. Potential barriers and wells are assumed to be evenly spaced in units of electrical distance (*dotted lines*).

mechanism leads to a countercurrent of ions and waters within the channel. Streaming potential measurements, however, suggest that one or two waters per ion move through the channel in the same direction as the ions (Alcayaga et al., 1989). (*b*) A second possibility is that an ion or molecule, or perhaps a sidechain of a channel protein, occupies the vacated space by moving in from the side of the channel wall. Such a mechanism is certainly conceivable and could lead to the general model of single-vacancy conduction. (*c*) The third possibility is that the vacated space is immediately filled by a neighboring ion in the conduction pore, along with any associated waters of hydration. This is the assumption of the present model. It is consistent with simulations of the dynamics of ions and waters within the conducting pore of the gramacidin channel (Mackay et al., 1984; Chiu et al., 1989; Jordan, 1990). These suggest that movements of ions and water within the conduction pore are highly correlated.

In Fig. 2 *b*, potential energy profiles of the three states of the shaking stack conduction mechanism are shown.

For each state, the channel is represented as a series of potential energy barriers separating potential energy wells. The wells correspond to localized binding sites within the conduction pore. This picture is motivated by the results of Neyton and Miller (1988*a*, *b*), who found evidence for localized sites with very high affinity for $K^+$ within the conduction pore of the rat skeletal CaK channel. The ions in each diagram are shown as circles located at the binding sites. If only three ions occupy the conduction pore, the strong affinity of the binding sites prevents further ions from escaping. This is suggested in the two lower diagrams by the high potential energy barriers at the two ends of the pore. Translocation of the stack leads to transitions between these two diagrams. When a fourth ion occupies the pore, it destabilizes the stack, perhaps due to electrostatic repulsion. An ion quickly escapes, corresponding to a transition from the diagram at the top of the figure to one of the two below.

In the sections that follow, we will analyze a shaking stack model with $m$ ion binding sites and occupied by a stack of $m - 1$ or $m$ ions. To reduce the number of free parameters available, we assume that the potential energy profile is symmetric and that, for a given ionic species, all wells have the same affinity and internal barriers have the same height, as is depicted in Fig. 2 *b*. Furthermore, the barriers and wells are assumed to be evenly spaced in units of electrical distance. This model is analogous to the "simple pore" model of single ion conduction described by Läuger (1973) and extended to single-vacancy conduction by Schumaker and MacKinnon (1990). It would correspond to a series of chemically identical, evenly spaced ion binding sites within a symmetrical conduction pore. Our analysis of the flux ratio exponent contains several results for more general shaking stack models.

The shaking stack model assumes the existence of discrete configurations of the stack, corresponding to the three diagrams in Fig. 2 *b*. Transitions between these states are governed by first order or pseudo-first order rate constants, which are assumed to have an exponential dependence on the applied transmembrane electrical potential. The simple pore model further assumes that the energy of the stack can be decomposed into a sum of contributions from the individual ions; such a decomposition is implied in Fig. 2 *b*. A more general shaking stack model need not require that the stack energy be decomposable into contributions from individual ions. The potential energy profile could be pictured as similar to that for a two-site single-vacancy model.

The validity of discrete state models recently has been the subject of much discussion. The application of absolute rate theory (Glasstone et al., 1941) to transitions taking place in a condensed phase has been criticized on the grounds that the theory assumes that these transitions happen in the absence of collisions (Levitt, 1986; Cooper et al., 1988; Dani and Levitt, 1990). Stack translocation in the absence of collisions certainly seems problematic. However, if the barriers between the states in Fig. 2 *b* are at least several $k_BT$, so that ions crossing those barriers suffer many collisions for each successful transition, a discrete state model with an exponential dependence of transition rates on barrier heights will be recovered. This is the local equilibrium approximation and is due to the collisions setting up a Boltzmann distribution of particle energies (Dani and Levitt, 1990). This approach is supported by the findings of Neyton and Miller (1988*a*, *b*), which suggest that high affinity binding sites line the conduction pore of the CaK channel. Cooper et al. (1988) have studied the diffusion of charged particles over potential barriers. They demonstrated that this kind of discrete state approximation breaks down if the applied electric field is too strong. This is essentially because very strong fields significantly change the shape of the potential profile. Under these conditions, the assumptions of the shaking stack model may break down. The required field strength depends on the unknown barrier heights.

## CONDUCTANCE

In this section we will derive an equation for the conductance of the $m$-site shaking stack model. The starting point for the analysis is the state diagram shown in Fig. 3 *a*. Each state is depicted as a schematic pore with occupied or unoccupied sites shown explicitly on either side and dots indicating occupied states in between. State 0 shows the stack completely filled with ions. In state 1, a vacancy appears at the right-hand binding site, and in state 2, a vacancy appears at the left-hand binding site. This diagram is topologically identical to that of a single-vacancy model with two ion binding sites.

The flux of ions passing from side 1 to side 2 through the pore corresponds to the frequency of cycles counterclockwise around the loop, and the flux directed from side 2 to side 1 corresponds to the frequency of clockwise cycles. According to the King-Altman method (King and Altman, 1956; Plowman, 1972; Hill, 1977), the net flux of ions, $J$, passing through the membrane and directed toward side 2 is given by

$$J = D^{-1}(\pi^+ - \pi^-), \tag{3}$$

where $\pi^+ = k_0k_1k_2$ is the product of the rate constants directed counterclockwise around the loop in the direction of the flux $J$, and $\pi^- = l_0l_1l_2$ is the product of the rate constants directed clockwise around the loop. The subscripts of these rate constants refer to the state from which the transition is made. The denominator, $D$, is the sum of directional diagrams oriented toward each state: $D = D_0 + D_1 + D_2$. Expressions for these are given in Appendix A.

The simple pore model uses the following values for the rate constants:

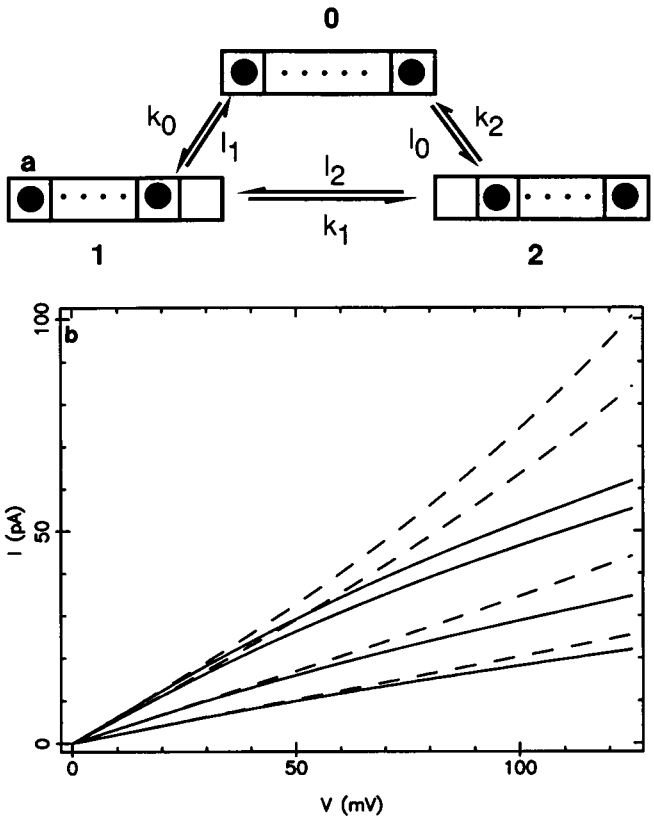


FIGURE 3 (*a*) State diagram for an *m*-site shaking stack conduction mechanism in the presence of a single permeant ion. Each rectangle schematically represents the single filing region of the conduction pathway. Individual ion binding sites are indicated by squares. Filled circles and ellipses between pairs of filled circles denote occupied sites. States 1 and 2 each have a single vacant ion binding site. Rate constants $k_i$ and $l_i$ are associated with transition between the states. (*b*) High curvature I-V curves corresponding to Eq. 7. Solid curves correspond to (−) rate constants and dashed curves correspond to (+) rate constants. At fixed $V$, increasing currents correspond to activities to 100, 200, 600, and 1,000 mM, respectively.

$$k_0 = be^{\nu}, \quad k_1 = ce^{(m-1)\nu}, \quad k_2 = x_1 ae^{\nu}, \quad l_0 = be^{-\nu},$$
$$l_1 = x_2 ae^{-\nu}, \quad l_2 = ce^{-(m-1)\nu}. \quad (4)$$

In the absence of a transmembrane potential, the (second-order) rate constant for an ion to enter the channel is $a$, the (first-order) rate constant for an ion to leave the channel is $b$, and the (first-order) rate constant for the stack to shift is $c$. When an electrical potential, $V$, is applied across the channel, rate constants are multiplied by a factor of $e^{\nu}$ when a single ion moves toward side 2 (either by entering the channel from side 1 or by exiting from the channel toward side 2), and the rate constant for stack transitions toward side 2, involving the concerted motion of $m - 1$ ions, is multiplied by a factor of $e^{(m-1)\nu}$. Rate constants are multiplied by corresponding factors of $e^{-\nu}$ and $e^{-(m-1)\nu}$ for ion motion in the direction of side 1. The exponent $\nu$ is the dimensionless electrical potential difference between a well and the barrier to its right: $\nu = zeV/2(m+1)k_BT$, where $z$ is the ion valence.

The conductance, $\gamma$, is given by $\gamma = (\partial I/\partial V)_0$. The final subscript (0) indicates that the derivative is evaluated at symmetric ion concentrations $x_1 = x_2 = x$ and zero transmembrane potential $V = 0$. The current, $I$, is related to the flux, $J$, by $I = zeJ$. The conductance can then be computed directly from Eq. 3, where the computation is simplified by noting that $(\pi^+ - \pi^-)_0 = 0$ by detailed balance. The result is

$$\gamma = \frac{z^2e^2}{k_BT}\frac{xabc}{(ax+2b)(ax+2c)} = \frac{z^2e^2}{k_BT}\frac{x}{A+Bx+Cx^2}, \quad (5)$$

where $A = 4a^{-1}$, $B = 2(b^{-1} + c^{-1})$, and $C = ab^{-1}c^{-1}$. This formula for the conductance of the $m$-site simple pore shaking stack model is formally independent of $m$; it is the same as that for the conductance of the single-vacancy model with two binding sites (Schumaker and MacKinnon, 1990).

## ANALYSIS OF CONDUCTANCE DATA

We are now in a position to analyze the conduction data presented in Results. The formulas below Eq. 5 may be inverted to give expressions for parameters of the simple pore shaking stack model in terms of the coefficients $A$, $B$, and $C$. We obtain

$$a = 4/A, \quad b_\pm = r_\pm, \quad c_\pm = r_\mp, \quad (6)$$

where $r_+ = (B + \Delta^{1/2})/AC$ and $r_- = (B - \Delta^{1/2})/AC$ are the roots of a quadratic equation with discriminant $\Delta = B^2 - 4AC$. In this notation, taking the top sign of ± gives one possible set of rate constants, which will be termed the (+) set, and the bottom sign gives the other possible set of rate constants, termed the (−) set. Substituting in the values for the high curvature parameters, we find $a = 1.69\ 10^9\ M^{-1}\ s^{-1}$, $r_+ = 4.07\ 10^9\ s^{-1}$, and $r_- = 3.36\ 10^8\ s^{-1}$. Corresponding values for the low curvature parameters are $a = 2.08\ 10^9\ M^{-1}\ s^{-1}$, $r_+ = 6.74\ 10^{10}\ s^{-1}$, and $r_- = 2.54\ 10^8\ s^{-1}$.

The values of the high curvature rate constants suggest that $b$ and $c$ are separated by a factor of ≥10, although they do not suggest which has the high value. As the curvature coefficient, $C$, decreases, the separation of $b$ and $c$ becomes even greater. The dependence of the rate constants on $C$ can be determined from an expansion of $\Delta^{1/2}$, which shows that the expressions for $r_+$ and $r_-$ simplify when $4AC/B^2 \ll 1$. Then we have $r_+ \approx 2B/AC$ and $r_- \approx 2/B$. We see that very small values of $C$ imply the existence of a high value for the rate constant $r_+$ in the conduction mechanism.

For comparison, some information about realistic time scales of molecular events is available. Molecular relaxation measurements, using high frequency sound absorption, suggest that the substitution rates of waters in the innermost hydration shell of the $K^+$ ion in aqueous solution are about $10^9\ s^{-1}$ (Eigen, 1963; Hille, 1992). The dielectric relaxation time of water, which is

thought to represent the lifetime of interwater hydrogen bonding, is about $10^{-11}$ s. In this connection, we note that stack translocation, which involves the concerted movement of ions and waters within the conduction pathway, may not require the disruption of $H_2O$-$K^+$ bonding.

## CURRENT

The ion flux through a shaking stack channel may be found directly from Eq. 3, which was used previously to calculate conductance. In Appendix A, the simple pore rate constants, Eq. 4, are substituted into Eq. 3. We are especially interested in the case $m = 4$, which the results of Neyton and Miller (1988*a*, *b*) suggest is of particular relevance to the calf skeletal muscle $Ca^{2+}$-activated $K^+$ channel. We then obtain

$$J = \frac{2xabc \sinh 5\nu}{2c(xa + b)\cosh 4\nu + 2b(xa + c)\cosh 2\nu + x^2a^2}. \quad (7)$$

The shape of the corresponding I-V curve can be conveniently analyzed by calculating $\sigma = (\partial^3 J/\partial \nu^3)_0$. When $\sigma < 0$, the current will be sublinear, and when $\sigma > 0$, it will be superlinear. The full expression for $\sigma$ is given by Eq. A4. From that formula, one immediately sees that the sign of $\sigma$ is the same as the sign of $25x^2a^2 + xa(26b - 46c) - 20bc$. At sufficiently small activities, the term $-20bc$ dominates, so that $\sigma < 0$ and the I-V curve is sublinear (at least, in a neighborhood of $V = 0$). At very high activities, the term $25x^2a^2$ dominates, so that $\sigma > 0$ and the curve is superlinear. Between these two regimes, $\sigma(x)$ must have a root. Applying the quadratic formula, one finds that there is a single positive root $x_+$ given by

$$x_+ = \{(23c - 13b) + [(23c - 13b)^2 + 500bc]^{1/2}\}/25a. \quad (8)$$

When $x < x_+$, the I-V curve is sublinear, and when $x > x_+$, it is superlinear.

Fig. 3 *b* shows I-V curves at four activities for the (+) and (−) sets of high curvature parameters. In the (+) case, there is a transition from sublinearity to superlinearity at $x_+ = 166$ mM. In the (−) case, $x_+ = 4.3$ M and the I-V curve is sublinear at all attainable activities. The roots of $\sigma$ for the low curvature parameters are $x_+ = 94$ mM for the (+) set and $x_+ = 59.5$ M for the (−) set.

The currents generated by the (−) parameter sets are qualitatively consistent with $K^+$ I-V curves published by Eisenman et al. (1986) in their study of the CaK channel from rat muscle. Those authors measured I-V curves at several values of symmetrical ion activity for each of four permeant ions—$K^+$, $Rb^+$, $Tl^+$, and $NH_4^+$. They found that the currents for $K^+$ and $Tl^+$ were sublinear, whereas those for $Rb^+$ and $NH_4^+$ were superlinear. In all cases, the sense of sub- or superlinearity was independent of ion activity. The agreement of the (−) parameter sets with the observed superlinearity of the $K^+$ current suggests that $c \gg b$, and hence stack translocation is the fastest first-order reaction step.

Although the consistency between the I-V curve shapes and the shaking stack model predictions is suggestive, the sublinearity of the $K^+$ and $Tl^+$ currents could be due to other causes (Yellen, 1984). One possibility is current saturation due to the access resistance of the electrolyte on either side of the membrane (Läuger, 1976). A second possibility is the breakdown of the exponential dependence of transition rates on the applied transmembrane electrical potential at high voltages (Cooper et al., 1988).

## REVERSAL POTENTIAL

One method for estimating the extent to which an ion channel selects between two permeant ion species is to measure the transmembrane potential required to maintain zero net current through the channel under "bi-ionic conditions," that is, when the solution on one side of the membrane contains one of the permeant species and the solution to the other side of the membrane contains the second. The required potential is known as the bi-ionic reversal potential and shall be designated $V_R$. In this section we shall investigate properties of the reversal potential for the simple pore shaking stack model.

Suppose the two permeant species are designated 1 and 2. We shall assume that species 1 is present on side 1 of the membrane with activity $x_1$ and that the activity of species 2 on side 1 is negligible. Similarly, we assume that species 2 is present on side 2 of the membrane with activity $x_2$ and that the activity of species 1 on that side of the membrane is negligible. The entry of species 1 into the channel from side 2 can therefore be neglected and vice versa. This condition leads to the state diagram for the shaking stack model under bi-ionic conditions, which is shown in Fig. 4 *a*. In this figure, filled circles represent ion 1 and enter the pore from the left, whereas open circles represent ion 2 and enter the pore from the right. A species 1 ion can only enter the solution on side 2 by making the transition from state $-M - 2$ to state $-M$ on the diagram. The frequency of this transition, corresponding to the unidirectional flux $\vec{J}$, is equal to the frequency of counterclockwise cycles around the bottom loop. Similarly, a species 2 ion only enters the solution on side 1 by making the transition from state $M + 2$ to state $M$, and the frequency of this transition, corresponding to the unidirectional flux $\overleftarrow{J}$, is equal to the frequency of clockwise cycles around the top loop.

The bi-ionic state diagram for the shaking stack model is similar in structure to that for the single-vacancy model (Schumaker and MacKinnon, 1990; see Fig. 4). The differences are that the top and bottom loops of the shaking stack state diagram contain only three states and that the "bridge" region connecting the loops is shorter. In effect, all of the states of the single-vacancy model that

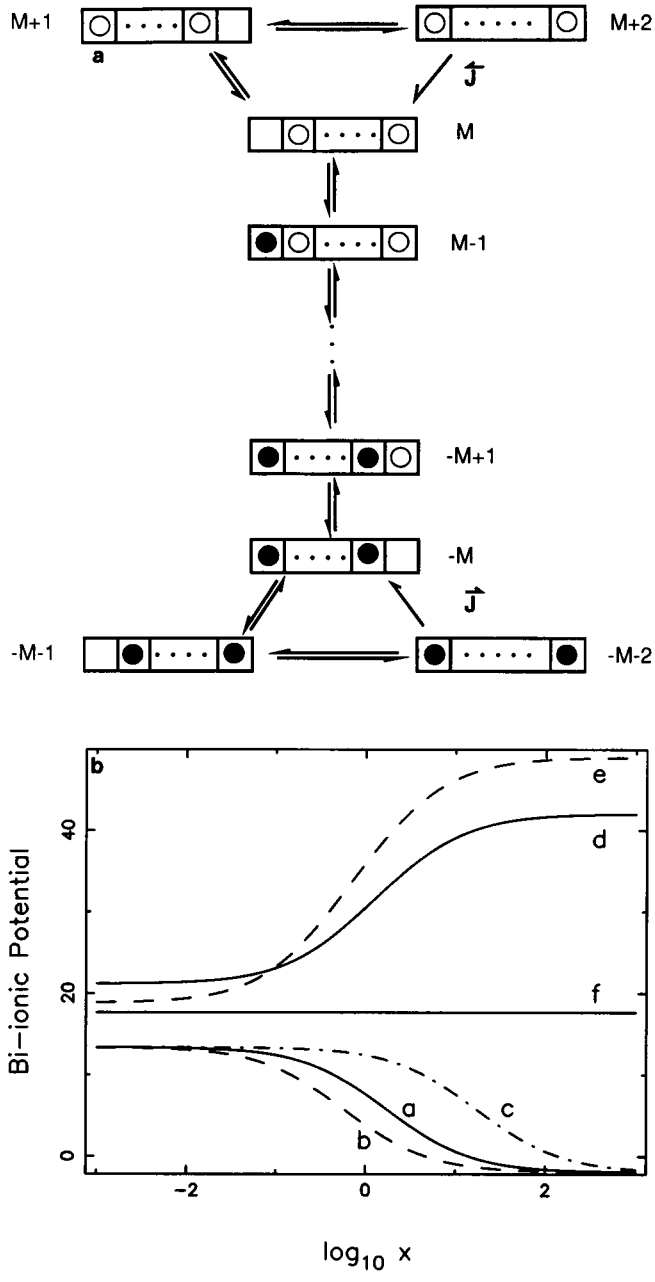


FIGURE 4 (*a*) State diagram for the shaking stack conduction mechanism under bi-ionic conditions. Filled circles represent ion 1 and enter the pore from the left. Open circles represent ion 2 and enter the pore from the right. States are numbered symmetrically from the middle of the bridge region between the two loops; $M = (3m - 4)/2$ ($m$ even) or $(3m - 3)/2$ ($m$ odd). There is a zero state only if $m$ is even. The unidirectional flux $\vec{J}$ corresponds to the rate of transitions between states $M + 2$ and $M$, and the flux $\overleftarrow{J}$ corresponds to the rate of transitions between states $-M - 2$ and $-M$. (*b*) Shaking stack reversal potential, $V_R$, as a function of $x_1 = x_2 = x$. Parameter values are given in units of $10^8\ M^{-1}\ s^{-1}$ for rate constant $a$ and $10^8\ s^{-1}$ for rate constants $b$ and $c$: (curve *a*) $m = 4$, $a_1 = 10$, $b_1 = 20$, $c_1 = 20$, $a_2 = 10$, $b_2 = 10$, $c_2 = 2$; (curve *b*) simple pore single-vacancy model with same parameters; (curve *c*) $m = 4$, $a_1 = 10$, $b_1 = 20$, $c_1 = 200$, $a_2 = 10$, $b_2 = 10$, $c_2 = 20$; (curve *d*) $m = 4$, $a_1 = 10$, $b_1 = 30$, $c_1 = 2$, $a_2 = 10$, $b_2 = 10$, $c_2 = 10$; (curve *e*) $m = 3$, $a_1 = 10$, $b_1 = 30$, $c_1 = 2$, $a_2 = 10$, $b_2 = 10$, $c_2 = 10$; (curve *f*) $m = 4$, $a_1 = 10$, $b_1 = 50$, $c_1 = 10$, $a_2 = 10$, $b_2 = 20$, $c_2 = 5.0297$. These cases are interpreted in the text.

involve vacancies interior to the endmost binding sites have been deleted.

To simplify calculations, we specialize to the case of the simple pore model. For ion 1 and in the absence of a transmembrane potential difference $V$, we assign a second-order rate constant $a_1$ for entrance into the channel, a first-order rate constant $c_1$ for translocation of the stack, and a first-order rate constant $b_1$ for exit from the stack. Corresponding rate constants for ion 2 are $a_2$, $c_2$, and $b_2$. In the presence of a potential $V$, the rates for individual ions to make transitions toward side 2 are multiplied by a factor of $e^{\nu}$, and the rates of transitions toward side 1 are multiplied by a factor of $e^{-\nu}$. Stack transition rates are multiplied by corresponding factors of $e^{(m-1)\nu}$ and $e^{-(m-1)\nu}$.

The bi-ionic reversal potential, $V_R$, is given implicitly by $\vec{J}(V_R) = \overleftarrow{J}(V_R)$. Expressions for $\vec{J}$ and $\overleftarrow{J}$ in terms of the rate constants defined above are developed in Appendix B. The calculations parallel those for the single-vacancy model. The reversal potential does not depend on any specific interactions, e.g., attraction or repulsion, between the ion species 1 and 2. The cancellation of these interactions is demonstrated in Appendix B for a particular choice of rate constants for translocation of stacks composed of both ions 1 and 2. However, this cancellation is a property of the general shaking stack model. A proof can be given that is similar to that developed by Schumaker and MacKinnon (1990) for the single-vacancy model.

We find simple analytical expressions for the solution $\underline{V_R}$ in the limit of low activities $c_1 \gg x_1 a_1$ and $c_2 \gg x_2 a_2$, as well as the solution $\overline{V_R}$ in the limit of high activities $x_1 a_1 \gg c_1$ and $x_2 a_2 \gg c_2$. These are given by

$$\underline{V_R} = \frac{k_B T}{ze}\left[\ln\frac{x_2}{x_1} + \ln\frac{a_2}{a_1} + \frac{m-1}{m}\ln\frac{b_1}{b_2}\right], \tag{9}$$

$$\overline{V_R} = \frac{k_B T}{ze}\left[\ln\frac{x_2}{x_1} + \ln\frac{a_2}{a_1} + \ln\frac{b_1}{b_2} + \frac{1}{m-1}\ln\frac{c_2}{c_1}\right]. \tag{10}$$

It is remarkable that these limiting reversal potentials are identical with those derived for the simple pore single-vacancy model!

Fig. 4 *b* shows several features of the shaking stack reversal potential when specialized to the simple pore model. We may have either $\overline{V_R} > \underline{V_R}$ or $\underline{V_R} > \overline{V_R}$. In any case, the reversal potential is always a monotonic function between the low and high activity limits. The proof parallels the one found in Schumaker and MacKinnon (1990) for the simple pore single-vacancy model. As the number of binding sites $m$ in the channel increases, the differences between $\overline{V_R}$ and $\underline{V_R}$ decrease; consider curves *d* and *e*. In the special case that $(m - 1)\ln b_2/b_1 = m \ln c_2/c_1$, the reversal potential is a constant function of the absolute concentration $x$; see curve *f*.

The transition from the low to high activity limits reflects a competition between the rate constants $c$ and $ax$.

This is reflected by curves $a$ and $c$ in Fig. 4 $b$. The parameters specifying these curves are the same except for the rate constants $c$. Each value of $c$ specified for curve $c$ is a factor of 10 greater than the corresponding value used to construct curve $a$. As a result, curve $c$ is shifted by 1 logarithm unit toward higher activities. Otherwise, the two curves are identical. Algebraically, the competition between $ax$ and $c$ determines which terms dominate in the expressions for $Q_1$ and $Q_2$, defined in Appendix B.

Blatz and Magleby (1984) measured reversal potentials in experiments with $K^+$ and $Rb^+$ under bi-ionic conditions. They found no apparent change in $V_R$ for symmetrical concentrations up to 500 mM, corresponding to activities of 325 mM for $K^+$ and 317 mM for $Rb^+$. Assuming that a transition from $V_R$ to $\overline{V_R}$ would be apparent at a $K^+$ activity $x_K$ satisfying $a_K x_K = c_K$, we can estimate from these data a lower bound for the $K^+$ rate constant $c_K$. Using an entrance rate constant of $a = 2\ 10^9$ $M^{-1}$ s for $K^+$, which is in the range of values given in the Analysis of Conductance Data, we find that $c$ can be no less than $\sim 6 \times 10^8\ s^{-1}$ to maintain consistency with the observations (excluding the exceptional case typified by the curve $f$ in Fig. 4 $b$). This lower bound apparently excludes the (+) sets of rate constants for both the high curvature and low curvature parameters. However, the (−) sets of rate constants are consistent with the lower bound. Assuming that the shaking stack model is qualitatively correct, the data thus suggest that Blatz and Magleby made their measurements in the low activity regime of $V_R$.

Fig. 4 $b$ also provides a comparison of the activity dependence of $V_R$ between a simple pore shaking stack model (curve $a$) and a simple pore single-vacancy model with the same rate constants $a$, $b$, and $c$ (curve $b$). These curves have the same high and low activity limits, consistent with the Eqs. 9 and 10 above. However, the transition between these limits for the single-vacancy model is shifted to lower activities as compared with that of the shaking stack model. This reflects the more efficient transport of vacancies across the channel via the shaking stack mechanism relative to the single-vacancy mechanism.

A frequently used measure of ion selectivity is the permeability ratio measured under bi-ionic conditions. In the Nernst-Planck theory of electrodiffusion, the permeability is defined as the ion flux across a membrane divided by the difference in ion concentrations driving the flux. The permeability for this theory is given by the Goldman-Hodgkin-Katz equation:

$$\frac{P_2}{P_1} = \frac{x_1}{x_2} \exp\left(\frac{V_R z e}{k_B T}\right) \tag{11}$$

(Goldman, 1943; Hodgkin and Katz, 1949). This expression is now used as an operational definition of the permeability ratio when experimental data are interpreted. Inserting the formula for $V_R$ from Eq. 9 into 11, we find the permeability ratio in the low activity limit:

$$\frac{P_2}{P_1} = \frac{a_2 b_2^{(1-m)/m}}{a_1 b_1^{(1-m)/m}}. \tag{12}$$

Similarly, the equation for the permeability ratio in the high activity limit is found from Eq. 10:

$$\frac{P_2}{P_1} = \frac{a_2 b_2^{-1} c_2^{1/(m-1)}}{a_1 b_1^{-1} c_1^{1/(m-1)}}. \tag{13}$$

These are again identical to the expressions found in the case of the single-vacancy channel. We note, in particular, that the permeability ratio in the low activity limit is independent of the translocation rate constants $c_1$ or $c_2$. In the limit as $m$ becomes large, it is the energy of ion binding at the potential energy wells that determines the permeability ratio.

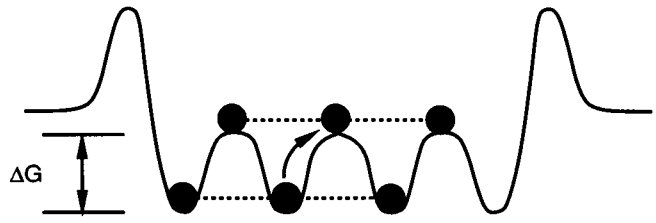


FIGURE 5 Stack translocation under the assumption that ions interact independently with barriers. The total barrier to stack motion is $3\Delta G$.

## SELECTIVITY

Conductance ratios and permeability ratios are two different measures of selectivity. The shaking stack model offers an interpretation of the mechanism of selectivity, which we can relate to conductance and permeability. To begin this interpretation, we make the very simple assumption that the ions interact with the chemical groups lining the pore independently (except for the fact that the ions in a stack move synchronously). This leads to the picture of Fig. 5. The figure shows separate energy barriers to the motion of individual ions in the stack. We assume that the effective barrier to translocation of the stack is the sum of these individual barriers. If the height of the internal barriers for ion 1 is $\Delta G_1/k_B T$, then a rate theory expression for the chemical part $c$ of the translocation rate constant would have the form

$$c_1 = c_1^0 \exp[-(m-1)\Delta G_1/k_B T], \tag{14}$$

where $c_1^0$ is a frequency prefactor. A similar expression would hold for ion 2. The ratio of these two rate constants is then

$$\frac{c_1}{c_2} \propto \exp[-(m-1)(\Delta G_1 - \Delta G_2)/k_B T]$$
$$= (\exp[-(\Delta G_1 - \Delta G_2)/k_B T])^{m-1}. \tag{15}$$

That is, the concerted motion of the stack multiplies the difference in activation energies for individual ions to

cross a barrier by $m-1$, raising the ratio of the translocation rate constants to the power $m-1$! Thus, the shaking stack conduction mechanism becomes more selective as the stack grows larger, and small differences between the chemical properties of ions become magnified. This may explain why evolution has selected for multi-ion channels.

Our assumption that the ions in a stack interact with the channel walls independently is convenient because it allows us to draw a potential energy diagram with individual barriers as in Fig. 5. However, the interpretation of selectivity made in the last paragraph does not depend on this assumption. Suppose, instead, that the height of the barrier to stack translocation depended on the length of the stack, perhaps because of the necessity for ions to coordinate with chemical groups spaced a fixed distance apart along the wall of the channel. The most conductive ion would result in a stack of ideal length. A small difference between the hydrated length of this ion and that of a different permeant ion would then be multiplied by the number of ions in the stack to give a total mismatch in stack length. This mechanism also leads to a selectivity advantage of long stacks.

Eisenman et al. (1986) found that the CaK channel selected very strongly in favor of $K^+$ over $Tl^+$, $Rb^+$, or $NH_4^+$ as judged by conductance ratios but that $Tl^+$ permeability was larger than that of $K^+$, and $Rb^+$ was only slightly less permeant. If the stack translocation rate constant, $c$, is the main arbiter of selectivity, then the shaking stack model offers an explanation for why conductance ratios should be greater than permeability ratios. Conductance ratios do depend on $c$ (Eq. 5). In the low activity regime, permeability ratios do not (Eq. 12).

## FLUX RATIO EXPONENT

In 1949 Ussing demonstrated that when ions diffuse freely across a membrane, the ratio of their unidirectional fluxes, $\vec{J}/\overleftarrow{J}$, depends on activity and transmembrane potential in a simple way, independent of the detailed membrane structure. Hodgkin and Keynes (1955) found that $K^+$ fluxes across the membrane of the cuttle fish giant axon violated Ussing's equation. This motivated their introduction of the flux ratio exponent $n$. This exponent describes how $\vec{J}/\overleftarrow{J}$ varies with the dimensionless electrochemical potential difference, $\Delta\mu$, across the membrane

$$\vec{J}/\overleftarrow{J} = e^{-n\Delta\mu}, \tag{16}$$

where

$$\Delta\mu = \mu_2 - \mu_1 = \ln\frac{x_2}{x_1} - \frac{zeV}{k_BT}. \tag{17}$$

Here, $x_1$ and $x_2$ represent the activities of a single permeant ion on the two sides of the membrane. The flux ratio exponent may be conveniently calculated for the

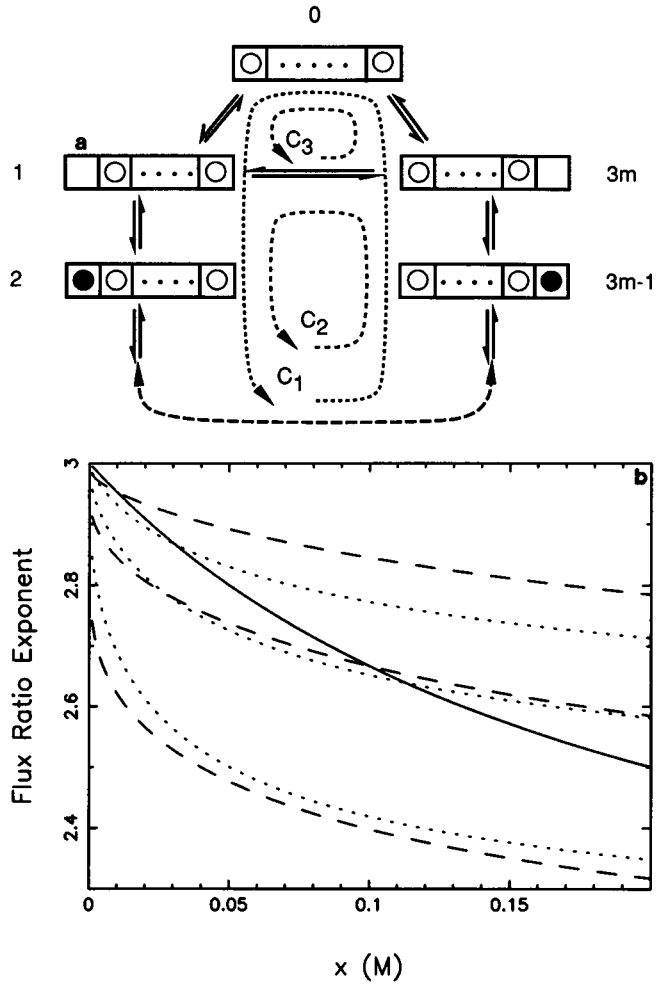


FIGURE 6 ($a$) State diagram for the shaking stack model in the presence of a second permeant ion at very small activity. The open circles denote the standard ion and the filled circles denote the tracer. Cycles $C_1$, $C_2$, and $C_3$ are shown, with the arrows indicating their positive sense. ($b$) Flux ratio exponent, $n$, shown as a function of activity $x$ for a simple pore shaking stack. Rate constants used are $a = 10^9\ s^{-1}$ and $c = 10^8\ s^{-1}$, giving $x_0 = 0.2$ M. The solid curve shows $n$ as a function of absolute activity, $x_1 = x_2 = x$, with $V = 0$, and follows Eq. 20. The dashed curves show $n$ as a function of relative activity, following Eq. 21. In order of descending values of $n$, these curves correspond to $x_1 = 0.01, 0.1$, and 1.0. In each case, $x_2 = x$ and $V = 0$. The dotted curves are perturbed from the corresponding dashed curves by a transmembrane potential of $V = -100$ mV. They follow Eq. 18.

shaking stack model by using a method developed by Kohler and Heckmann (1979). Those authors calculated the exponent for the single-vacancy model. Suppose that two isotopes of a permeant ion exist, the "standard" isotope and a "tracer" isotope. The tracer is present in solution at such a small activity that the probability that two tracer particles will occupy the channel at the same time is negligible. These assumptions lead to the state diagram shown in Fig. 6 $a$. Transitions around the cycle $C_3$ correspond to the permeation of standard ions only through the pore. Transitions around the cycle $C_2$ correspond to ion permeation with a

single tracer occupying the pore. The largest cycle, $C_1$, is a sum of the other two. The state diagram for the single-vacancy model would include states with internal vacancies in the cycle $C_2$. These do not appear in the present state diagram for the shaking stack conduction mechanism.

The analysis of Kohler and Heckmann (1979) leads to an implicit equation for the flux ratio exponent. As discussed in Appendix C, we may solve this explicitly for $n$, and further simplify the result in special cases. We obtain:

$$n = m - \frac{1}{2} + \frac{1}{\Delta\mu} \ln\left\{\frac{1 + \alpha e^{\Delta\mu/2}}{\alpha + e^{\Delta\mu/2}}\right\}, \tag{18}$$

where

$$\alpha = \frac{2c}{a x_1^{1/2} x_2^{1/2}} \cosh \nu. \tag{19}$$

Eq. 18 holds for a general $m$-site shaking stack model, that is, one with arbitrary rate constants and electrical distances. The form of Eq. 19 for $\alpha$ pertains to the simple pore model; however, the dependence on $x_1$ and $x_2$ shown agrees with the general case, and so the conclusions about the activity dependence of the flux ratio exponent discussed below will also hold in general.

We first discuss how $n$ depends on the absolute activity $x = x_1$, keeping the relative activity $r = x_2/x_1 \neq 0$ constant. In this case, $\Delta\mu$ is fixed, and $n$ depends on $x$ only through $\alpha$. Differentiating Eq. 18 with respect to $\alpha$, one finds that $(\partial n/\partial\alpha)_{\Delta\mu} > 0$. As $x$ increases from 0 to $\infty$, $\alpha$ decreases monotonically from $\infty$ to 0 and $n$ decreases monotonically from $m$ to $m - 1$. These results agree with Kohler and Heckmann's (1979) analysis of the activity dependence of $n$ in the general single-vacancy model. They are also consistent with Levitt's (1984) qualitative discussion of the single-vacancy exponent and competition between rates of ion entrance and translocation.

To determine how quickly $n$ decreases, we can take the limit of Eqs. 18 and 19 as $\Delta\mu \to 0$. Such a limit would correspond to hypothetical measurement of the flux ratio exponent under equilibrium conditions, that is, with no net current flowing through the channel. In practice, such a measurement cannot be undertaken because a finite current must exist to be observable. However, the limit will approximate measurements taken near equilibrium. The limiting formula for the flux ratio exponent is given in Appendix C. One conclusion from an analysis of this limit is that, with a given upper bound $x$ for attainable ion activity, $n$ has its least value when $x_1 = x_2 = x$ and $V = 0$. Under these conditions, the limit further simplifies and one obtains

$$n = m - \frac{x}{x_0 + x}. \tag{20}$$

For the simple pore model, $x_0 = 2c/a$; the dependence on $x$ holds in general. At low ion activities, $x \ll x_0$, the exponent $n$ will decrease linearly from $m$ as a function of $x$. At high activities, $x \gg x_0$, $n - (m - 1)$ halves as $x$ doubles. An example is given by the solid curve in Fig. 6 *b*.

Flux ratio exponents are often measured under conditions in which it is convenient to vary the activity of ions on only one side of the membrane. This corresponds to varying the relative activity, $r$, while holding the absolute activity, $x$, fixed. Both $\alpha$ and $\Delta\mu$ in Eq. 18 depend on $r$. Taking $V = 0$ in Eq. 18, the flux ratio exponent for an arbitrary shaking stack model is given by

$$n = m - \frac{1}{\ln r} \ln\left\{\frac{x_0 + xr}{x_0 + x}\right\}, \tag{21}$$

with the same $x_0$ as appears in Eq. 20. In contrast with the algebraic decay of $n$ with $x$, Eq. 20, the exponent depends logarithmically on the activity ratio. Three examples are shown by the dashed curves in Fig. 6 *b*. As $r$ increases from 0, $n$ decreases abruptly from $m$ with an initially infinite slope and then decreases ever more gradually. When $r > 1$ and $x_2 \gg x_0$, $n - (m - 1)$ halves as $\ln r$ doubles.

The transmembrane electrical potential, $V$, may also be controlled experimentally. The dotted curves in Fig. 6 *b* indicate that $n$ depends rather weakly on $V$ for the cases shown. Taking the limit of Eqs. 18 and 19 as $|V| \to \infty$, one finds, for the simple pore model,

$$V \to m - \frac{1}{2} + \frac{1}{2(m+1)} + \mathcal{O}\left(\frac{k_B T}{zeV}\right), \tag{22}$$

where $\mathcal{O}(v^{-1})$ denotes terms that approach 0 at least as fast as $v^{-1}$. If $m = 3$, then $n \to 2.625$. For a general shaking stack model, the limit of $n$ may be anywhere in the interval $(m - 1, m)$, depending on the distribution of electrical distances.

The analyses in this section can be compared with the measurements of Vestergaard-Bogind et al. (1985) on the flux ratio exponent $n$ of the Gárdos CaK channel in human red blood cells. The Gárdos channel has markedly asymmetric conduction properties, and its conductance in symmetrical $K^+$ is about an order of magnitude smaller that of the high conductance CaK channel (Christophersen, 1991). Two series of flux ratio exponent measurements were made, varying the transmembrane electrical potential over a range ($-100$ mV $\leq V_m \leq$ 0 mV) and the external $K^+$ concentration (1 mM $\leq [K^+]_{ex} \leq$ 150 mM). The results of both series of measurements were $n \approx 2.7$, apparently independent of both $V_m$ and $[K^+]_{ex}$. This suggests that the Gárdos channel has a very high affinity for $K^+$ ions, motivating a comparison with the shaking stack model. The observed constancy of $n$ may be consistent with the rather weak dependence that the shaking stack exponent can have on the relative ion activity, $r$, and transmembrane potential, $V$.

However, Vestergaard-Bogind et al. (1985) also made several measurements of $n$ with different intracellular

$K^+$ concentrations in the range of 30–145 mM (Stampe, P., personal communication) without observing a trend. These results remain difficult to explain.

## SUMMARY

Neyton and Miller (1988*a*, *b*) concluded that the conduction pore of CaK channels from rat skeletal muscle has four high affinity $K^+$ binding sites, at least three of which are occupied under normal conducting conditions. Vestergaard-Bogind et al. (1985) measured a constant flux ratio exponent in the CaK channel of the human red blood cells, indicating that this is also an "ion-avid" channel. These findings motivated the single-vacancy model of ion conduction (Schumaker and MacKinnon, 1990). The shaking stack mechanism is a variant of single-vacancy conduction that is suggested by a consideration of possible mechanisms for ion movement between the binding sites.

This paper develops a shaking stack model for a pore containing $m$ ion binding sites. The hydrated ions within the single filing region are assumed to form a stack of $m$ or $m-1$ ions, occupying a contiguous string of sites. A stack of $m-1$ ions has a vacancy at one end. It can make a transition in the direction of that vacancy, occupying the previously empty site and creating a vacancy at the other end of the stack. This concerted transition fulfills the requirement that the space left behind by a moving ion be immediately reoccupied by matter. Conduction occurs when an ion from solution occupies the vacant binding site at one end of the stack, destabilizing the stack, and allowing an ion from the other end to come off.

If the ions forming the stack interact with the channel walls independently, then the concerted motion of the stack will multiply the activation energies for an ion to cross a barrier between binding sites by a factor of $m-1$. The difference in activation energies between two stacks composed of different ions is then $m-1$ times the corresponding energy difference between individual ions. This greatly enhances the selectivity of the channel. Even if the interaction of the stack with the channel walls cannot be decomposed into individual ion contributions, the stack transition energy may still depend, in a very sensitive way, on the properties of its constituent ions.

The conductance, current, permeability ratio, and flux ratio exponent have been investigated analytically for a shaking stack model with a simplified set of rate constants. The conductance has the same form as that for a two-site single-vacancy model, with a maximum value at high symmetrical activities. When $m = 4$, the shape of the I-V curve can be conveniently analyzed for super- or sublinearity. At very low ion activities the curves will be sublinear, and at very high activities they will be superlinear. A simple formula has been found for the critical activity, $x_+$, which divides these two regions. The low and high activity limits of the reversal potential are the same as previously found for the single-vacancy model. In particular, the permeability ratio at low activities does not depend on the height of the energy barrier to stack translocation. The flux ratio exponent, $n$, decreases from $m$ at low activities to $m-1$ at high activities. The decrease will be most marked in experiments conducted at symmetrical ion activities.

A set of conductance data was analyzed to determine the range of parameter values required to duplicate the properties of the CaK channel. The rate constants for stack translocation and ion exit must be separated by a factor of $\sim 10$ or more to account for the absence of a definitive curvature in the graph of $x/\gamma$ as a function of $x$. A comparison of possible model parameter sets with the conductance and current data reported by Eisenman et al. (1986) and the reversal potential measurements of Blatz and Magleby (1984) suggests that stack translocation is the fast rate process. Qualitative agreement was then established with several findings of those authors.

Finally, a comparison was made with the flux ratio exponent measurements of Vestergaard-Bogind et al. (1985) on the Gárdos CaK channel of human red blood cells. The apparent insensitivity of the exponent $n$ to the investigated range of transmembrane potentials and relative ion activities reported may be consistent with the weak dependence that the shaking stack exponent can have with respect to these parameters. However, those authors have also made several measurements of $n$ with different intracellular $K^+$ concentrations without observing a trend. These results have not been explained.

## APPENDIX A

In this appendix, expressions for the current and conductance of the shaking stack model will be derived. A formula for $\sigma$, related to the shape of the I-V curve, is also given.

The general expression for the current is given by Eq. 3, where the rate constants defined in Eq. 4 are used. Evaluating the numerator under conditions of symmetrical ion concentrations, we have $\pi^+ = xabce^{(m+1)\nu}$ and $\pi^- = xabce^{-(m+1)\nu}$. According to the King-Altman method, the denominator is the sum of three terms, $D = D_0 + D_1 + D_2$, where $D_i$ is the directional diagram directed toward state $i$. In terms of rate constants,

$$\begin{aligned} D_0 &= l_1l_2 + l_1k_2 + k_1k_2, \\ D_1 &= l_2l_0 + l_2k_0 + k_2k_0, \\ D_2 &= l_0l_1 + l_0k_1 + k_0k_1. \end{aligned} \tag{A1}$$

Inserting the values of the rate constants corresponding to the simple pore model, Eq. 4, we obtain

$$J = \frac{2xabc \sinh (m+1)\nu}{2(xac + bc)\cosh m\nu + 2bc \cosh (m-2)\nu + 2xab \cosh 2\nu + x^2a^2}. \tag{A2}$$

The case $m = 4$ is given by Eq. 7. With $m = 2$, this formula agrees with the expression obtained for the current through a two-site single-vacancy model (Schumaker and MacKinnon, 1990). A direct comparison may be made by multiplying the numerator and denominator of Eq. A2 by $\sinh \nu$ and then using an identity to expand the denominator.

The conductance, $\gamma$, evaluated at symmetric ion concentrations and zero transmembrane potential, is given by:

$$\gamma = \left.\frac{\partial I}{\partial V}\right|_0 = ze\left.\frac{\partial J}{\partial V}\right|_0 = \frac{z^2e^2}{2(m+1)k_BT}\left.\frac{\partial J}{\partial v}\right|_0. \quad \text{(A3)}$$

Differentiation of Eq. A2 leads to Eq. 5.

The shape of the I-V curve for $m = 4$ may be characterized by $\sigma = (\partial^3 J/\partial v^3)_0$. This is computed by direct differentiation of Eq. 7. The expressions obtained are fairly simple because many of the terms vanish when $v$ is set to zero. One finds

$$\sigma = \frac{10xab(25x^2a^2 + 26xab - 46xac - 20bc)}{(xa + 2b)^2(xa + 2c)^2}. \quad \text{(A4)}$$

Regarded as a function of $x$, $\sigma$ has three roots: one is negative, one is zero, and the root $x_+$, given by Eq. 8, is positive.

## APPENDIX B

In this appendix we will sketch the calculation of the reversal potential for the shaking stack model. The reversal potential, $V_R$, is the solution of $\vec{J}(V_R) = \overleftarrow{J}(V_R)$. $\vec{J}$ is equal to the frequency of transitions clockwise around the top loop in Fig. 4 *a*. According to the King-Altman method (see Hill, 1977, chapter 2), the frequency of clockwise transitions around the top loop is given by the product of rate constants clockwise around that loop, multiplied by a sum of products of rate constants, each product corresponding to a tree in the remaining portion of the diagram directed toward the top loop. $\overleftarrow{J}$ is calculated in an analogous way. In equations, $\vec{J}(V_R) = \overleftarrow{J}(V_R)$ may be written in the following form:

$$Q_1B_{12}\pi_2 = Q_2B_{21}\pi_1. \quad \text{(B1)}$$

Here $\pi_1$ is the product of rate constants counterclockwise around the bottom loop in Fig. 4 *a*, and $\pi_2$ is the product of rate constants clockwise around the top loop. Substituting in the simple pore rate constants, described in the Reversal Potential, we have:

$$\pi_1 = x_1a_1b_1c_1e^{(m+1)v}, \quad \pi_2 = x_2a_2b_2c_2e^{-(m+1)v}. \quad \text{(B2)}$$

$B_{12}$ signifies the product of rate constants up the bridge, from the bottom loop to the top loop, and $B_{21}$ signifies the product of rate constants down the bridge:

$$B_{12} = x_2^{m-1}a_2^{m-1}b_1^{m-1}\left(\prod_{i=1}^{m-2} d_i\right)e^{-m(m-1)v}, \quad \text{(B3)}$$

$$B_{21} = x_1^{m-1}a_1^{m-1}b_2^{m-1}\left(\prod_{i=1}^{m-2} d_i\right)e^{m(m-1)v}. \quad \text{(B4)}$$

In these expressions, the rate constant $d_i$ pertains to the rate of translocation of a stack composed of $i$ ions of type 1 and $m - 1 - i$ ions of type 2.

The assumption that these rates depend only on the total composition of the stack and not on the arrangement of ions within the stack is arbitrary. However, when Eqs. B3 and B4 are inserted into Eq. B1, we see that the rate constants $d_i$ cancel out. This is an instance of the general rule that all specific interactions between the two different species of ions cancel out in the calculation of the reversal potential. The general proof of this fact is completely analogous to that given for the single-vacancy model by Schumaker and MacKinnon (1990), and depends on the fact that only a single bridge of states connects the two cycles in the diagram. The proof also requires that all rate constants depend exponentially on the transmembrane potential, $V$.

The expression for $Q_1$ is given by summing together all products of rate constants corresponding to ways that transitions can be directed from the states of the bottom loop toward the top loop. Conversely, the expression for $Q_2$ is given by summing the ways that transitions from the top loop can be directed toward the bottom loop. These combinations are given by the following expressions:

$$Q_1 = b_1(c_1e^{-mv} + c_1e^{-(m-2)v} + x_1a_1e^{2v}), \quad \text{(B5)}$$

$$Q_2 = b_2(c_2e^{mv} + c_2e^{(m-2)v} + x_2a_2e^{-2v}). \quad \text{(B6)}$$

The result for $V_R$, corresponding to the limit $c_1 \gg x_1a_1$ and $c_2 \gg x_2a_2$, is obtained by neglecting the last terms in Eqs. B5 and B6 and then inserting Eqs. B2 through B6 into B1. On canceling terms and solving the remainder for $V_R$, Eq. 9 is obtained. Conversely, the result for $\overline{V}_R$, corresponding to the limit $x_1a_1 \gg c_1$ and $x_2a_2 \gg c_2$ is obtained by neglecting the first two terms in Eqs. B5 and B6 and then inserting Eqs. B2 through B6 into B1. Solving for $V_R$, Eq. 10 is obtained.

## APPENDIX C

The method of Kohler and Heckmann (1979) is used to calculate the flux ratio exponent from Fig. 6 *a*. This state diagram differs slightly from that considered by those authors. The general single-vacancy model has states in the cycle $C_2$, with vacancies at the internal binding sites, which are not present in the shaking stack model. However, this does not change their method. We obtain a result in the form given by Kohler and Heckmann,

$$e^{-n\Delta\mu} = \frac{\vec{J}}{\overleftarrow{J}} = \frac{e^{-(m-1)\Delta\mu} + \rho e^{-m\Delta\mu}}{1 + \rho}. \quad \text{(C1)}$$

This holds for a general shaking stack model. For the simple pore model, $\rho = (2c/x_1a)e^{-(m+1)v}\cosh v$.

We can further analyze this result by solving explicitly for $n$. Put Eq. C1 into a symmetrical form with respect to the low and high activity limits of the flux ratio exponent by defining $\alpha = e^{-\Delta\mu/2}\rho$. The flux ratio is then given by the expression

$$\frac{\vec{J}}{\overleftarrow{J}} = e^{-(m-1/2)\Delta\mu}\left\{\frac{e^{\Delta\mu/2} + \alpha}{1 + \alpha e^{\Delta\mu/2}}\right\}. \quad \text{(C2)}$$

Solving for $n$, we obtain Eqs. 18 and 19.

To calculate the limit of the right-hand side of Eq. 18 as $\Delta\mu \to 0$, expand $x_1$ and $x_2$ about reference values: $x_1 = x_1^0 + \xi_1$ and $x_2 = x_2^0 + \xi_2$. If $V_N = (k_BT/ze)\ln x_2^0/x_1^0$ is the Nernst potential associated with these reference activities, then the dimensionless electrical potential drop, $v_N$, between a binding site and an adjacent potential energy barrier will be given by $2(m + 1)v_N = \ln x_2^0/x_1^0$. The applied electrical potential may also be expanded about $v_N$: $v = v_N + \delta$. Assuming that $\xi_1$, $\xi_2$, and $\delta$ are all of first order in smallness, we can expand the logarithm on the right hand side of Eq. 18 to obtain

$$\lim_{\Delta\mu\to 0}\frac{-1}{\Delta\mu}\ln\left\{\frac{e^{\Delta\mu/2} + \alpha}{1 + \alpha e^{\Delta\mu/2}}\right\} = \frac{1}{2}\left(\frac{\alpha_0 - 1}{\alpha_0 + 1}\right), \quad \text{(C3)}$$

where, for a simple pore channel at a general Nernst equilibrium

$$\alpha_0 = \frac{2c}{a(x_1^0x_2^0)^{1/2}}\cosh v_N. \quad \text{(C4)}$$

Inserting this limit into the right-hand side of Eq. 18, we obtain

$$n = m - \frac{a(x_1^0x_2^0)^{1/2}}{a(x_1^0x_2^0)^{1/2} + 2c\cosh v_N}. \quad \text{(C5)}$$

For a given maximum value of the reference ion activities, the smallest value of $n$ will be measured when $x_1^0 = x_2^0$. This further simplifies the above formula, and we obtain Eq. 20.

The form of Eq. 20 may also be obtained for the general shaking stack

model (calculations not shown). When $x_1^0 = x_2^0 = x$, so that $\nu_N = 0$, we can write $\alpha_0 = x_0/x$, where $x_0$ has the dimensions of concentration. Inserting this into Eq. C3 and the result into Eq. 18, we again obtain Eq. 20.

I gratefully acknowledge many enjoyable and enlightening discussions with Roderick MacKinnon. These sparked the central idea of this paper. The data shown in Fig. 1 were taken in collaboration with Roderick MacKinnon and Christopher Miller, in the latter's lab at Woods Hole. Christopher Miller kindly reviewed this manuscript. I thank Per Stampe for discussing the flux ratio exponent and sharing his unpublished results. Finally, I am grateful to Toshiko Ichiya, Jim Satterlee, and Scott Wherland for helpful conversations concerning realistic rates of physical processes that might be involved in ion conduction.

This investigation was supported in part by funds provided by Washington State University.

*Received for publication 16 September 1991 and in final form 23 March 1992.*

## REFERENCES

Alcayaga, C., X. Cecchi, O. Alvarez, and R. Latorre. 1989. Streaming potential measurements in $Ca^{2+}$-activated $K^+$ channels from skeletal and smooth muscle. *Biophys. J.* 55:367–371.

Andersen, O. S., and J. Procopio. 1980. Ion movement through gramacidin A channels. *Acta Physiol. Scand. Suppl.* 481:27–35.

Blatz, A., and K. Magleby. 1984. Ion conductance and selectivity of single calcium-activated potassium channels in cultured rat muscle. *J. Gen. Physiol.* 84:1–23.

Chiu, S.-W., S. Subramanian, E. Jakobsson, and J. A. McCammon. 1989. Water and polypeptide conformations in the gramacidin channel. *Biophys. J.* 56:253–261.

Christophersen, P. 1991. $Ca^{2+}$-Activated $K^+$ channel from human erythrocyte membranes: single channel rectification and selectivity. *J. Membr. Biol.* 119:75–83.

Cooper, K. E., P. Y. Gates, and R. S. Eisenberg. 1988. Diffusion theory and discrete rate constants in ion permeation. *J. Membr. Biol.* 106:95–105.

Dani, J. A., and D. G. Levitt. 1990. Diffusion and kinetic approaches to describe permeation in ionic channels. *J. Theor. Biol.* 146:289–301.

Eigen, M. 1963. Fast elementary steps in chemical reaction mechanisms. *Pure Appl. Chem.* 6:97–115.

Eisenman, G., R. Latorre, and C. Miller. 1986. Multi-ion conduction and selectivity in the high-conductance $Ca^{++}$-activated $K^+$ channel from skeletal muscle. *Biophys. J.* 50:1025–1034.

Gárdos, G. 1958. The function of calcium in the potassium permeability of human erythrocytes. *Biochim. Biophys. Acta.* 30:653–654.

Glasstone, S., K. J. Laidler, and H. Eyring. 1941. The Theory of Rate Processes. McGraw-Hill Inc., New York. 611 pp.

Goldman, D. E. 1943. Potential, impedance and rectification in membranes. *J. Gen. Physiol.* 27:37–60.

Hill, T. L. 1977. Free Energy Transduction in Biology. Academic Press, New York. 229 pp.

Hille, B. 1992. Ionic Channels of Excitable Membranes, 2nd Ed. Sinauer Assoc. Inc., Sunderland. 280 pp.

Hodgkin, A. L., and B. Katz. 1949. The effect of sodium ions on the electrical activity of the giant axons of the squid. *J. Physiol. (Lond.).* 108:37–77.

Hodgkin, A. L., and R. D. Keynes. 1955. The potassium permeability of a giant nerve fiber. *J. Physiol. (Lond.).* 128:61–88.

Jordan, P. C. 1990. Ion-water and ion-polypeptide correlations in a gramacidin-like channel. *Biophys. J.* 58:1133–1156.

King, E. L., and C. Altman. 1956. A schematic method of deriving the rate laws for enzyme-catalyzed reactions. *J. Phys. Chem.* 60:1375–1378.

Kohler, H.-H., and K. Heckmann. 1979. Unidirectional fluxes in saturated single file pores of biological and artificial membranes I. Pores containing no more than one vacancy. *J. Theor. Biol.* 79:381–401.

Latorre, R., and C. Miller. 1983. Conduction and selectivity in potassium channels. *J. Membr. Biol.* 71:11–30.

Latorre, R., C. Vergara, and C. Hildago. 1982. Reconstitution on planar lipid bilayers of a $Ca^{2+}$-dependent $K^+$ channel from transverse tubule membranes isolated from rabbit skeletal muscle. *Proc. Nat. Acad. Sci. USA.* 77:7484–7486.

Läuger, P. 1973. Ion transport through pores: a rate theory analysis. *Biochim. Biophys. Acta.* 311:423–441.

Läuger, P. 1976. Diffusion-limited ion flow through pores. *Biochim. Biophys. Acta.* 455:493–509.

Läuger, P. 1980. Kinetic properties of ion carriers and channels. *J. Membr. Biol.* 57:163–178.

Levitt, D. G. 1984. Kinetics of movement in narrow channels. *Curr. Top. Membr. Transp.* 21:182–197.

Levitt, D. G. 1986. Interpretation of biological ion channel flux data: reaction rate versus continuum theory. *Annu. Rev. Biophys. Biophys. Chem.* 15:29–57.

Mackay, D. H. J., P. H. Berens, K. R. Wilson, and A. T. Hagler. 1984. Structure and dynamics of ion transport through gramacidin-A. *Biophys. J.* 46:229–248.

MacKinnon, R., R. Latorre, and C. Miller. 1989. Role of surface electrostatics in the operation of a high-conductance $Ca^{2+}$-activated $K^+$ channel. *Biochemistry.* 28:8092–8099.

Miller, C. 1987. Trapping single ions in single ion channels. *Biophys. J.* 52:123–126.

Moczydlowski, E., and R. Latorre. 1983. Saxitoxin and oubain binding activity of isolated skeletal muscle membrane as indicators of surface origin and purity. *Biochim. Biophys. Acta.* 732:412–420.

Neyton, J., and C. Miller. 1988*a*. Potassium blocks barium permeation through a calcium-activated potassium channel. *J. Gen. Physiol.* 92:549–567.

Neyton, J., and C. Miller. 1988*b*. Discrete $Ba^{2+}$ block as a probe of ion occupancy and pore structure in the high-conductance $Ca^{2+}$-activated $K^+$ channel. *J. Gen. Physiol.* 92:569–586.

Plowman, K. M. 1972. Enzyme Kinetics. McGraw-Hill Inc., New York. 171 pp.

Schumaker, M. F. 1991. The shaking stack model of ion conduction through the $Ca^{++}$-activated $K^+$ channel. *Biophys. J.* 59:77a.

Schumaker, M. F., and R. MacKinnon. 1990. A simple model for multi-ion permeation. *Biophys. J.* 58:975–984.

Ussing, H. H. 1949. The distinction by means of tracers between active transport and diffusion. *Acta Physiol. Scand.* 19:43–56.

Vestergaard-Bogind, B., P. Stampe, and P. Christophersen. 1985. Single-file diffusion through the $Ca^{2+}$-activated $K^+$ channel of human red blood cells. *J. Membr. Biol.* 88:67–75.

Villarroel, A., and G. Eisenman. 1987. Surface charge in a barrier model can explain the low concentration I-V behavior of the $Ca^{++}$-activated $K^+$ channel. *Biophys. J.* 51:546a.

Yellen, G. 1984. Ionic permeation and blockade in $Ca^{2+}$-activated $K^+$ channels of bovine chromaffin cells. *J. Gen. Physiol.* 84:157–186.